Chapter 10
Modelling Void Growth to Coalescence in a 3-D Particle Field

10.1 Void Growth and Shape Evolution

Modeling of the growth and shape evolution of the voids and cracks in the percolation model requires certain assumptions since the evolution models are designed for spheroids and not for general 3-D ellipsoids. The main challenge in adapting these models to the general case is their implicit dependence upon the loading direction. By assuming a periodic distribution of axisymmetric voids, the void aspect ratio can be defined as a state variable with a definitive initial value that can evolve during deformation. However, in the general case, the loading direction is not constrained to a specific direction and the aspect ratio is not an independent variable, but a function of the loading direction. This point is best illustrated if we consider a penny-shaped void that has just nucleated from a cracked particle. If the principal loading direction happens to be aligned with the opening direction of the void, it will appear as a penny-shaped void as viewed from the loading direction and there is no issue. If the loading direction happens to be transverse to the void opening direction, the penny-shaped void appears as an extremely prolate or needle-shaped void that will experience negligible growth and shape evolution. Certainly the void growth and shape evolution rules for a penny-shaped void do not apply in this case.

With this in mind, all void/crack growth and shape evolution will be governed by the principal loading direction and how the geometry of the void appears from this direction. The development of general three-dimensional void evolution models that explicitly accounts for the viewing direction would be a welcome contribution to the percolation model.

Z. Chen and C. Butcher, *Micromechanics Modelling of Ductile Fracture*,
Solid Mechanics and Its Applications 195, DOI 10.1007/978-94-007-6098-1_10,

10.2 Procedure for Modeling Void Growth and Shape Evolution

Eliminating the void aspect ratio as a state variable requires the determination of the void dimensions and shape relative to the principal loading direction. Consider an arbitrary void or crack with the semi-axes (a, b, c) corresponding to the vectors $\mathbf{n}_1$, $\mathbf{n}_2$, $\mathbf{n}_3$. The principal loading direction is defined by the vector $\boldsymbol{u}$, as seen in Fig. 10.1. The distance from the center of the void to its surface along the direction $\boldsymbol{u}$, is denoted R_1. A line-projection of the void is then taken with $\boldsymbol{u}$ as the viewing direction to obtain an ellipse with semi-axes R_2 and R_3 that coincide with the $\boldsymbol{p}$ and $\boldsymbol{n}$ directions. The reconstructed geometry of the void as viewed from the principal loading direction is an ellipsoid with semi-axes, R_1, R_2, R_3 and the equivalent aspect ratio is defined as

$$W = \frac{R_1}{\sqrt{R_2 R_3}} \tag{10.1}$$

This aspect ratio is used to evaluate the void growth and shape evolution models but the porosity of the actual void is used in these models and not the porosity of the equivalent void.

The void growth and shape evolution rates can now be determined from knowledge of this effective aspect ratio. The void growth rate, $\dot{f}/f$, is determined using the calibrated void growth rule of Ragab (2004b) using the unit cell correlations obtained in Chap. 4. Similarly, the evolution rate of the effective void aspect ratio, $\dot{W}/W$, is also determined using the unit cell correlations in Chap. 4. These evolution rates were obtained for the equivalent void and are not truly representative of the actual void since these growth rates are not aligned with the semi-axes of the actual void. A clever application of the unit cell geometric relationships from Chap. 4

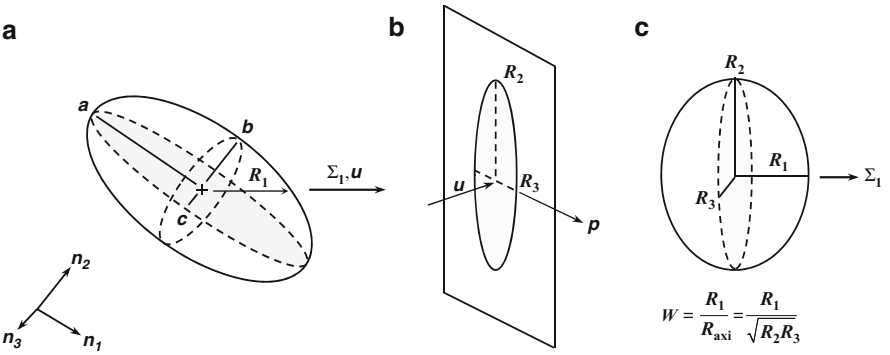

Fig. 10.1 Procedure for modeling an arbitrary ellipsoidal void as an axisymmetric void as viewed by the principal loading direction. (**a**) Ellipsoidal void, (**b**) void projection and (**c**) model ellipsoidal void

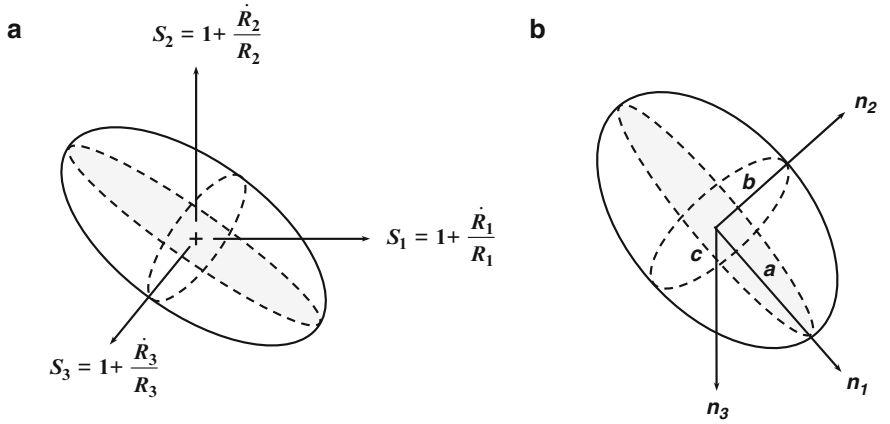

Fig. 10.2 Stretching of a void in three arbitrary directions resulting in a new void size and orientation. (**a**) Stretching of the void in the u, p, n directions and (**b**) new void size and orientation

enable the calculation of the radial growth rates of the equivalent axisymmetric void as a function of the principal strain rates as

$$\frac{\dot{R}_1}{R_1} = \dot{E}_{\text{hyd}} + \frac{1}{3}\left(\frac{\dot{f}}{f} + 2\frac{\dot{W}}{W}\right) \tag{10.2}$$

$$\frac{\dot{R}_2}{R_2} = \frac{\dot{R}_3}{R_3} = \frac{\dot{R}_1}{R_1} - \frac{\dot{W}}{W} \tag{10.3}$$

The evolution rates of the equivalent void semi-axes are taken as the growth rates of the actual void but in the directions $\boldsymbol{u}, \boldsymbol{p}, \boldsymbol{n}$. The problem can now be treated as the stretching of an ellipsoid along three arbitrary directions as shown in Fig. 10.2. The stretch values of the void in the $\boldsymbol{u}, \boldsymbol{p}, \boldsymbol{n}$ directions are

$$S_1 = 1 + \frac{\dot{R}_1}{R_1} \qquad S_2 = 1 + \frac{\dot{R}_2}{R_2} \qquad S_3 = S_2 \tag{10.4a, b, c}$$

The solution for the arbitrary stretching of an ellipsoid requires an eigenvalue solution where the eigenvalues are related to the new void semi-axes with their orientation defined by the eigenvectors. The solutions for the line projection of an ellipsoid, the distance from an ellipsoid center to its surface and for the arbitrary stretching of an ellipsoid are presented in Butcher (2011).

The novelty of this modeling procedure is that the evolution of the void orientation is naturally accounted for in the model, and this is not captured using the standard growth and shape models in the literature. The void will naturally grow and rotate itself to be aligned with the preferential loading direction. If the

directions of the semi-axes and principal loading directions are aligned, the void will not rotate. Additionally, the growth and shape evolution rates are calculated using the library of unit cell correlations and therefore provide very good estimates for the evolution rates.

10.3 Void Coalescence

As with void growth and shape evolution, departing from a periodic microstructure containing axisymmetric voids in favour of a general distribution of 3-D ellipsoids introduces challenges for void coalescence modeling. The plastic limit-load coalescence model has been widely used in the literature as well as validated in Chap. 4. The model is robust and can give very strong predictions of coalescence if one happens to have two identical voids horizontally aligned transverse to the principal loading direction. Certainly, this is not the general case and some modifications are required to utilize this criterion in the percolation model. Butcher and Chen (2009a, b, c) have appended the plastic limit-load model in a prior 2-D version percolation model. Scheyvaerts et al. (2010) considered the possibility of coalescence on angles in a periodic microstructure in plane strain tension with shear. The modeling of void coalescence in a general particle field will be separated into four categories that require consideration:

Determination of the stress state when the voids are located in different elements
Identification of the coalescence plane and appropriate stress transverse to the arbitrarily oriented ligament
Determination of the spacing ratio and equivalent void geometry for two arbitrary ellipsoidal voids
Merging procedure to create the coalesced crack (void)

10.3.1 Coalescence Between Elements

The stress state within each percolation element is assumed to be uniform since the presence of the voids and particles are not explicitly modeled in the finite-element program. Therefore, if the coalescence criterion is to be evaluated for two voids located in different parent elements, the average stress tensor of the elements is computed as

$$\Sigma_{ij}^{c} = \frac{\Sigma_{ij}^{e1} + \Sigma_{ij}^{e2}}{2} \tag{10.5}$$

This is a rather simplistic approach to estimating the stress tensor in the region between the two elements; however, it is reasonable if the element resolution is

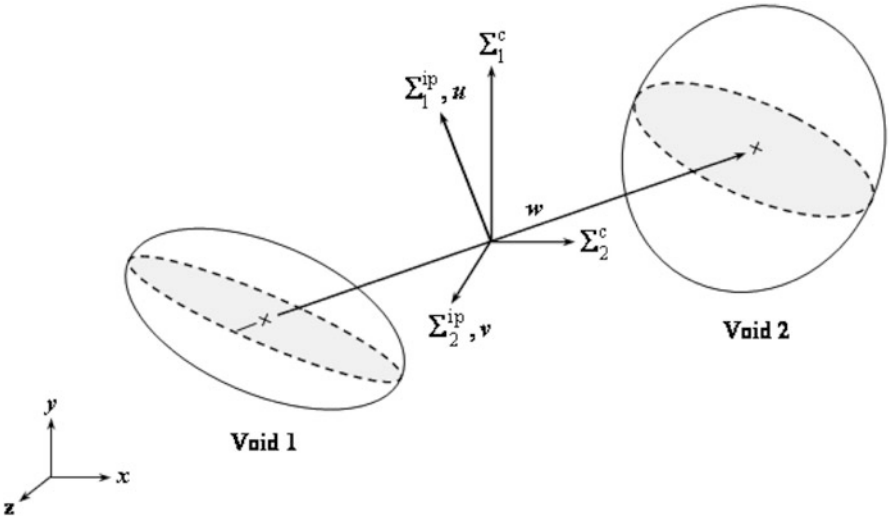

Fig. 10.3 Void coalescence geometry showing the in-plane tensile stress values transverse to the inter-void ligament vector, w

such that the variation in the stress state between elements is small. Future work could take advantage of the integration points within the element to better estimate the stress in a specific region of the element.

10.3.2 Identification of the Maximum Stress Transverse to the Ligament

The plastic limit-load coalescence model assumes that the neighbouring voids are aligned so that the center-to-center vector is transverse to the maximum principal stress. Obviously this is not the general case and this condition must be relaxed to be applied for a general void distribution.

First, consider two arbitrary ellipsoidal voids subjected to an arbitrary loading where the principal loading direction is not transverse to the inter-void ligament as defined by the center-to-center vector, $\boldsymbol{w}$, in Fig. 10.3. In a two-dimensional model, a simple stress transformation can be used to obtain the stress transverse to the ligament and the evaluation of the criterion can proceed. In the three-dimensional case, a plane exists that is transverse to the ligament and the stress will vary within this plane. The maximum tensile stress within this plane must be determined to evaluate the plastic limit-load criterion. This stress will be referred to as the 'maximum in-plane tensile stress' and is denoted, Σ_1^{ip}. The second in-plane stress that is transverse to both Σ_1^{ip} and the ligament is denoted, Σ_2^{ip}.

The in-plane stresses can be determined by selecting an arbitrary coordinate system using the vectors $\boldsymbol{u}$, $\boldsymbol{v}$, and $\boldsymbol{w}$. Within this plane exists an angle, θ, that will rotate $\boldsymbol{u}$ and $\boldsymbol{v}$ about $\boldsymbol{w}$ to be aligned with the in-plane stress vectors. The solution for these vectors has been framed as an optimization problem to enable its extension in future work to minimize the plastic limit-load by accounting for the variation in the dimensions of the voids as a function of θ. For an assumed vector, $\boldsymbol{v} = [v_1,v_2,v_3]$, and center-to-center vector, $\boldsymbol{w} = [w_1,w_2,w_3]$, the trial in-plane stress is defined using a vector, $\boldsymbol{s} = [s_1,s_2,s_3]$, as a function of θ by

$$\Sigma_1^{ip}(\theta) = s^T \Sigma_{ij}^c s \tag{10.6}$$

$$\begin{aligned}
s_1 &= \left(v_1^2 + (1 - v_1^2)\cos\theta\right)w_1 + (v_1 v_2(1 - \cos\theta) - v_3 \sin\theta)w_2 \\
&\quad + (v_1 v_3(1 - \cos\theta) + v_2 \sin\theta)w_3 \\
s_2 &= (v_1 v_2(1 - \cos\theta) + v_3 \sin\theta)w_1 + \left(v_2^2 + (1 - v_2^2)\cos\theta\right)w_2 \\
&\quad + (v_2 v_3(1 - \cos\theta) - v_1 \sin\theta)w_3 \\
s_3 &= (v_1 v_3(1 - \cos\theta) - v_2 \sin\theta)w_1 + (v_2 v_3(1 - \cos\theta) - v_1 \sin\theta)w_2 \\
&\quad + \left(v_3^2 + (1 - v_3^2)\cos\theta\right)w_3
\end{aligned}$$

An iterative Newton–Raphson search quickly converges to the solution by iterating with respect to θ. The value of θ in the *n-th* + 1 iteration is

$$\theta_{n+1} = \theta_n - \frac{d\Sigma_1^{ip}(\theta)/d\theta}{d^2\Sigma_1^{ip}(\theta)/d\theta^2} \tag{10.7}$$

Once θ has been determined, the vectors $\boldsymbol{u}$ and $\boldsymbol{v}$ can be rotated to the optimal directions and the in-plane stress values can be determined using the standard stress transformations

$$\Sigma_1^{ip} = u^T \Sigma_{ij}^c u \qquad \Sigma_2^{ip} = v^T \Sigma_{ij}^c v \tag{10.8}$$

In many cases, void coalescence will be triggered by the maximum in-plane tensile stress but coalescence can also occur in the second in-plane stress direction depending on the void alignment and stress state. It is cautioned that a preoccupation with the maximum tensile stress governing coalescence can lead to erroneous predictions in equal-biaxial stretching when $\Sigma_2^{ip} \approx \Sigma_1^{ip}$. In the interest of being conservative, coalescence will also be evaluated in the second in-plane stress direction whenever $\Sigma_2^{ip} > 0$. Knowledge of the tensile stress along the vector, $\boldsymbol{w}$, is not important even in triaxial loading since the void spacing ratio will be zero as the voids are aligned in this direction and the plastic limit-load to coalescence will be infinite. This type of coalescence is rare and is known as ‘necklace’ coalescence and cannot be predicted by the plastic limit-load model.

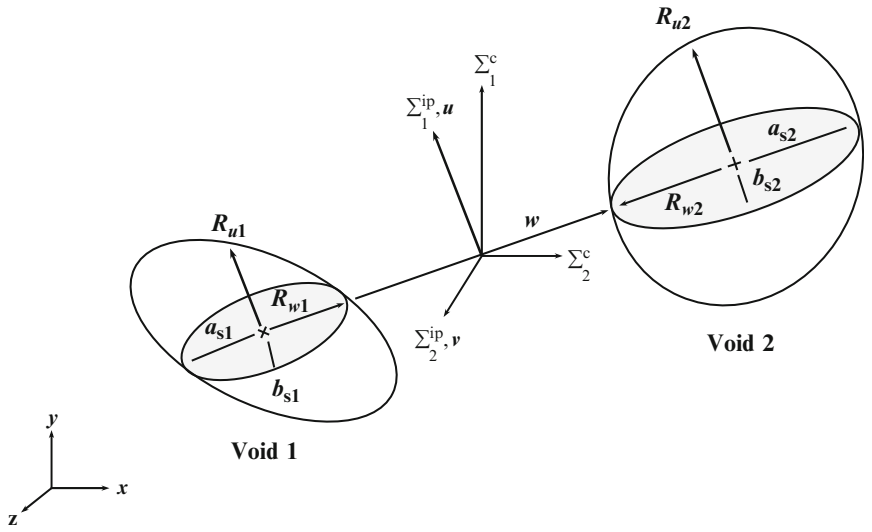

Fig. 10.4 Void coalescence geometry showing the identification of the relevant dimensions

10.3.3 Effective Geometry for the Evaluation of Coalescence

A procedure must be developed to effectively homogenize the two voids into an equivalent geometry of two identical voids to be amenable to the evaluation of the coalescence model. The plastic limit-load criterion requires knowledge of the void aspect ratio, W, spacing ratio, χ, and the maximum tensile stress transverse to the ligament. The maximum in-plane tensile stress has been determined in the optimization procedure above. The void spacing ratio is readily determined from the center-to-center distance, $d_{c2c} = \|x_{c1} - x_{c2}\|$, between the void centroids, $\boldsymbol{x}_{\mathrm{ci}}$, as

$$\chi_c = \frac{R_{w1} + R_{w2}}{d_{c2c}} \tag{10.9}$$

where R_{w1} and R_{w2} are the distances from the voids, measured from their center to their surface along the center-to-center vector, $\boldsymbol{w}$, as seen in Fig. 10.4. The center-to-center distance is used for modeling coalescence so that the spacing ratio reduces to its original definition in the plastic limit-load formulation when the voids are aligned and have the same orientation. It is important to state that χ_{c} in Eq. (10.9) is not the absolute minimum spacing ratio between the two voids. The minimum spacing ratio is not employed because it is computationally expensive and requires an iterative solution for every void-neighbour pair in every element at each time step. Overall, the center-to-center spacing ratio is a good approximation to the minimum spacing ratio provided the voids are not very close together and have similar orientations.

The principal approximations and uncertainties introduced into the coalescence model are related to the determination of the equivalent aspect ratio. The voids have arbitrary sizes and orientations and are far from the idealized geometry of two identical spheroidal voids. The aspect ratio of the equivalent axisymmetric void is defined as

$$W_{eq} = \frac{R_u}{R_{axi}} \tag{10.10}$$

where R_u is the radius along the in-plane stress direction and R_{axi} is the equivalent axisymmetric radius. The height of the equivalent spheroidal void, R_u, can be estimated by averaging the distance from the void centers to their surfaces along the in-plane stress direction as

$$R_u = \frac{R_{u1} + R_{u1}}{2} \tag{10.11}$$

To determine the equivalent axisymmetric radius, each void is first sectioned transverse to the in-plane stress direction to obtain an ellipse with semi-axes (a_{si}, b_{si}) as shown in Fig. 10.4. For clarity, R_{w1} and R_{w2} are shown to be aligned with the section of the ellipse in Fig. 10.4 but the semi-axes of the sectioned ellipsoid are generally not equal to the R_w distance due to the void orientation.

Since the locations of the semi-axes in the section planes may be different for the two voids, these dimensions cannot be directly averaged. Instead an equivalent axisymmetric radius is defined for each void as

$$R_{1-axi} = \sqrt{a_{s1} b_{s1}} \quad R_{2-axi} = \sqrt{a_{s2} b_{s2}} \tag{10.12}$$

and the axisymmetric radius of the equivalent void and its aspect ratio are computed as

$$R_{axi} = \frac{R_{1-axi} + R_{2-axi}}{2} \quad W_{eq} = \frac{R_{u1} + R_{u1}}{R_{1-axi} + R_{2-axi}} \tag{10.13, 10.14}$$

The coalescence criterion in Eq. (1.15) can now be evaluated using W_{eq}, χ_c, Σ_1^{ip}, and the matrix flow stress, $\bar{\sigma}$. The geometry of the voids used in the coalescence model is shown in Fig. 10.5.

10.3.4 Creation of a New Crack: Merging Operation

When the coalescence criterion is satisfied for two voids/cracks, a new crack must be created by merging the two voids together. The merging operation plays a significant role in the fracture process since the size of the resulting crack will

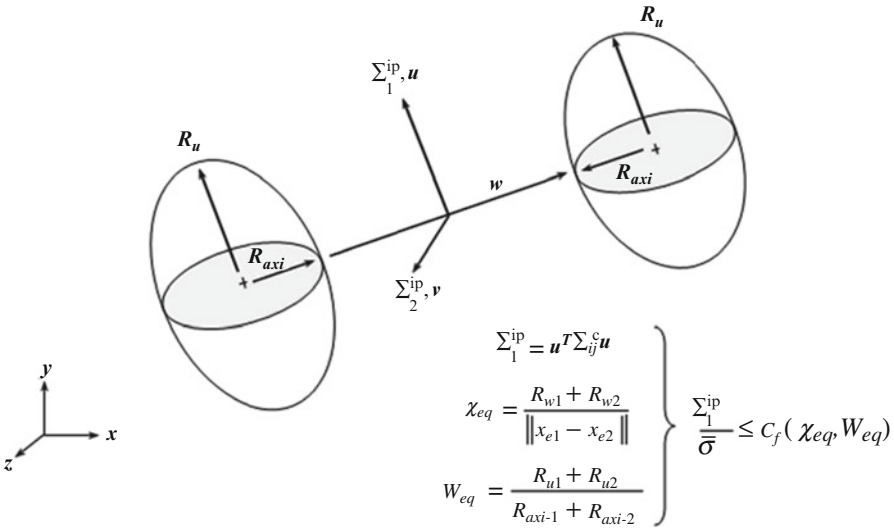

Fig. 10.5 Equivalent void geometry for evaluation of the plastic limit-load coalescence model

influence coalescence with other neighbouring voids. The simplest merging operation is to use the maximum void dimensions of the two voids to make a large crack that encompasses both voids as in Worswick et al. (2001). The disadvantage of this model is that the crack size is uncharacteristically large and coalescence quickly spreads throughout the particle field.

The bounding box method presented in Fig. 10.6 is used to define the new crack dimensions. The crack is assumed to be oriented with its semi-axes along the $\boldsymbol{u}$, $\boldsymbol{v}$, $\boldsymbol{w}$ vectors identified in the previous section for the in-plane stresses. The dimensions and points that will define the bounding box for the new crack must be identified in the three planes defined by $\boldsymbol{u}$, $\boldsymbol{v}$, $\boldsymbol{w}$. Each void bounding box will have four points that lie above and four points that lie below the plane and the distances from these points to the plane are calculated as D_{a1i}, D_{b1i} for void 1 and D_{a2i}, D_{b2i} for void 2. The semi-axis of the crack in this plane is then computed as

$$R = \frac{\max(D_{a1i}, D_{a2i}) + \max(D_{b1i}, D_{b2i})}{2} \quad i = 1 \ldots 4 \tag{10.15}$$

This process is repeated for each plane to obtain the three semi-axes of the crack. The center of the crack can be determined by constructing the bounding box for the crack by using one void centroid as the reference point. The centroid is the midpoint of the bounding box coordinates.

The maximum distances above and below the planes are employed to ensure that the crack will progressively enlarge as it coalesces with other voids and cracks. The average void dimensions could be used but only for void-void coalescence and not for void-crack or crack-crack coalescence as the amplification effect of the crack

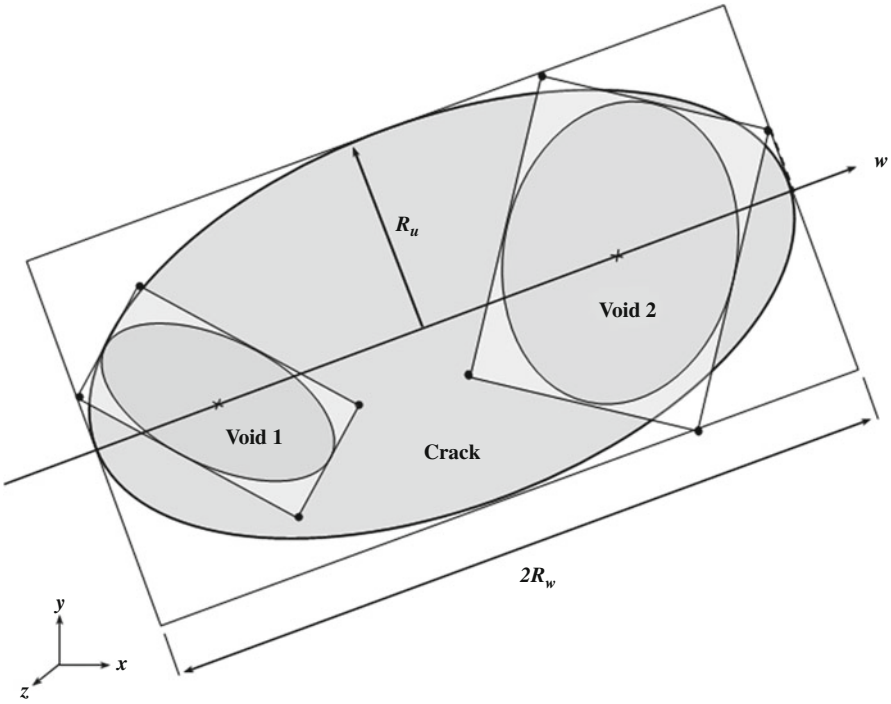

Fig. 10.6 Two-dimensional schematic of coalescence between two voids showing their bounding boxes and the creation of the new crack

size will be lost. If the voids that compose the crack belong to different parent elements, the parent element of the crack is identified as the element with the minimum distance from the element center to the crack centroid.

Overall, this merging procedure is about as good as one can achieve without resorting to an optimization algorithm to determine the minimum ellipsoid that envelops both voids. This merge procedure works very well for most void geometries except for coalescence between a large and small void where the crack size is overestimated as shown in Fig. 10.7. Fortunately, this does not become significant until large cracks have first formed which typically does not occur until prior to fracture when coalescence is sweeping throughout the element and failure is imminent. Nevertheless, future work could extend the merge operation to account for the relative sizes of the voids in determining the size of the new crack.

10.3.5 Mandatory Coalescence: Object Intersections

It is not uncommon for voids and cracks to overlap as they evolve with deformation or coalesce with their neighbours. This type of void/crack impingement is not realistic since the material between the voids will fail before the voids come into

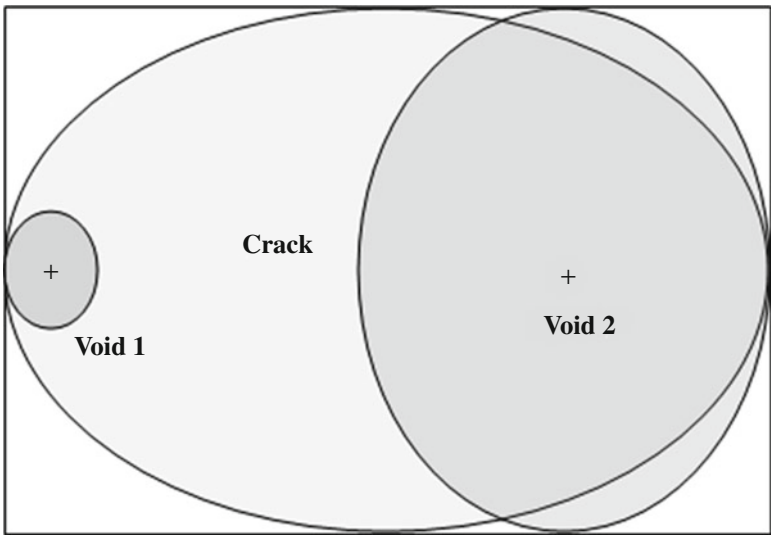

Fig. 10.7 Schematic of coalescence between a large and small void and the resulting crack geometry

contact (Thomason 1990). As a result, when a void or crack overlaps with another neighbouring void, the coalescence process is enforced using the merging process described above. The minimum distance algorithm of Lin and Han (2002) is evaluated prior to testing for coalescence at each time step. There are no restrictions placed upon particles coming into contact with voids, cracks or other particles for the sole reason of reducing the number of intersection tests. Each percolation element may contain thousands of particles and their overlapping is of secondary importance compared to the voids. A worthwhile extension would be to treat the particles as rigid bodies that cannot intersect to model the creation of deformation-induced particle clusters as the particles pile up with their neighbours. The proximity of a particle next to an existing crack would also promote premature void nucleation.

10.4 Development of the Percolation Model

In this chapter, the void growth and evolution models developed in the previous chapters are amalgamated into a complete framework to model damage evolution in a material with a heterogeneous particle distribution. The void evolution models are adapted to a general three-dimensional particle field and stress state by removing the periodic assumption used in their development in Chap. 5. The percolation model was then integrated into a commercial finite-element code, LS-DYNA (Hallquist 2006) to create so-called 'percolation elements' by mapping the particle distributions to the elements. This enables the percolation model to be directly coupled

to the macro-scale as damage evolution at the micron-scale will control the stress state in the elements, and ultimately, that of the entire structure via the FE method. This represents a significant contribution in the modeling of ductile fracture as the particle distribution can be accounted for in finite-element simulations of metal forming

The development of a sophisticated constitutive model of this scale requires careful consideration and justification of each step in the modeling process to ensure that the model has a strong physical foundation. The development of the percolation model will be separated into two main categories: macroscopic models and microscopic models. The macroscopic models are used to transition from the micro-scale to the macro-scale and vice versa.

10.4.1 Principal Assumptions

The principal advantage of the damage percolation model is that the microstructure no longer is assumed to be periodic and a measured particle/void distribution can be used to model ductile fracture. A concerted effort has been made in this work to improve the physical foundation of the percolation model and significant progress has been achieved in reducing the number of assumptions inherent in the modeling of ductile fracture. Nevertheless, extending the micromechanical models to a general three-dimensional case requires numerous approximations and assumptions. The principal assumptions used in the development of the percolation model are:

- The stress state within the element is uniform and homogeneous. Local stress and strain heterogeneity within void and particle clusters is neglected.
- The particles, voids and cracks do not interact. Voids/cracks grow as isolated voids.
- Void evolution models obtained using axisymmetric unit cells can provide a reasonable approximation to the growth of voids in a real material if the shear stress is small compared to the tensile stress.
- The particles, voids and cracks remain ellipsoidal during deformation.
- Nucleation via debonding is not explicitly modeled. An emphasis is placed upon void nucleation via particle cracking.
- Void coalescence occurs by necking failure of the inter-void ligament. Ligament shearing is not considered.
- Size effects are negligible at the length scales considered and continuum-based models for void initiation and evolution are valid at the micron-scale and higher. Deformation of voids and particles that are smaller than 1 μm would require considering dislocation dynamics.
- The grains and texture-related effects are not accounted for in the model. It is assumed that the bulk properties of the particle field are isotropic and rate-independent although deformation of the voids at the local-scale is dependent upon the loading direction.

Each of the above assumptions will introduce a degree of uncertainty into the model with the major limitations being the assumption of a uniform stress distribution, no shear coalescence, negligible size effects and neglecting anisotropy and the grains in the material. The rationale for these assumptions is discussed in the following sections.

10.4.1.1 Assumption of a Homogeneous Stress State – No Void and Particle Interactions

Although the stress state is assumed to be homogeneous within the percolation element, the stress state is not homogeneous because severe local strain-gradients develop within particle and void clusters. As a result, the voids and particles will interact and not evolve as isolated objects. This assumption is unlikely to be overcome without explicitly modeling every void and particle using finite-element techniques; however, it can be improved by using a sufficient number of percolation elements. In the limit, each percolation element would contain a single void/particle and the isolated assumption becomes realistic.

10.4.1.2 Assumption of Internal Necking Coalescence as the Dominant Coalescence Mode

The omission of a shear-based coalescence model is an unfortunate limitation of the present work and is attributed to the lack of a robust model akin to the plastic limit-load criterion for internal necking coalescence. Butcher and Chen (2009a) proposed a shear-extension to the plastic limit-load for combined tension and shear based upon the work of Xue (2008). However, this model is better suited for a general constitutive model and not for individual voids. A recent work by Schyvearts et al. (2011) has found that the plastic limit-load model can give good predictions for necking coalescence in combined tension and shear by accounting for the void orientation with shear. The percolation model is also expected to perform well in this situation as it accounts for the orientation of the voids and cracks as well as their rotation when they evolve and change shape in shear loading.

10.4.1.3 Assumption of Size-Effects Being Negligible Above the Micron-Scale

All multi-scale models are only valid for a range of length scales. The percolation model has been designed to model void initiation and evolution from the micron-scale to the macro-scale. The typical size of a second-phase particle in many alloys is on the order of several microns or larger in diameter. It is assumed that continuum-scale models can be used to describe the deformation of the particles and voids at this scale. Size effects are unavoidable and it is well known that sub-micron sized voids tend to grow slower than their larger counterparts (Liu et al.

2003; Tvergaard and Niordson 2004; Wen et al. 2005). At the sub-micron scale, dislocation dynamics must be considered using a strain-gradient plasticity model (Fleck and Hutchinson 1997) that includes a length scale parameter for the size effects. Fortunately, a numerical study by Wen et al. (2005) has found that the void size effect is limited in uniaxial tension and for a small volume fraction of voids. Since most metal forming operations occur in the low triaxiality regime ($T < 1$) and have failure porosities on the order of several percent at most, the size effect can be neglected as a first-order approximation of the material behavior. An extension of the percolation model that accounts for dislocation dynamics on void nucleation and evolution would improve the physical foundation of the model and enable it to incorporate events from the nano-scale to the macro-scale.

10.4.1.4 Neglecting the Influence of Texture Effects and Grains

The percolation model does not account for influence of material texture or for the presence of grains in the material. This assumption implies that it is the presence of the micro-voids in the material that are responsible for the promotion of localization and fracture. For example, in a uniaxial tensile test, geometric softening causes the material to form a localized neck. The stress state in the center of the necked region becomes severe and spurs void nucleation and growth, softening the material in the neck and causing additional necking. Ultimately, the sample fails as the voids coalesce throughout the necked region. This type of fracture mechanism can be well described using a damage-based approach such as the percolation model.

This type of fracture process is not always the case since anisotropy and the grain structure of the material can be responsible for the initial localization by the formation of shear bands. These shear bands provide the high local plastic strains required to drive void nucleation and growth, softening the material in the shear band and promoting additional localization until fracture occurs. In this situation, the isotropic percolation model would overestimate the strain and porosity at fracture since higher levels of porosity would be required to trigger the localization process without the presence of the shear bands.

Overall, the percolation model provides an excellent tool for the modeling of ductile fracture and can describe a large portion of the fracture process. A future extension of the percolation model should account for material anisotropy in the yield criterion and void evolution models. The influence of the grains could be accounted for by coupling the percolation model with a crystal plasticity model. The coupled crystal plasticity – percolation model would provide insight into the complete fracture process by accounting for the entire microstructure.

10.4.1.5 Terminology Used in Development of the Percolation Model

The particle field is assumed to be composed of particles/inclusions, voids and cracks and referred to as ‘objects’ if the modeling treatment is the same for each

constituent. Particles are modeled as a single class but their composition and type may be variable to accommodate different particle types in the material. Cracks are subjected to the same modeling treatments as voids but are defined as a crack to discriminate between the primary and nucleated voids with the voids that form due to coalescence. A crack is formed by the coalescence between a void and a crack, two voids or two cracks.

10.4.2 Macroscopic Models

Quantities at the element scale are defined as macroscopic because the stress state within the element is obtained by homogenizing the voids within the microstructure using the GT yield criterion. In this definition, the element is analogous to the typical unit cell except the cell contains a particle field instead of a single void. The purpose of the macroscopic modeling process is to accept the nodal displacements from the finite-element code and determine the stress and strain according to the adopted constitutive model for the element. The failure criterion for the element is then evaluated and the element is deleted or the stress returned to the finite-element solver. This is the typical procedure for any finite-element program with the only notable difference being that the constitutive model is rather complex. An overview of the macroscopic modeling process is presented in Fig. 10.8.

The elements provide the link to the relevant length scales for engineering (mm and higher) because the stress state within the elements controls the deformation of the global structure. Therefore, a brief review of the relevant kinematics of the finite-elements is required as they play a major role in the percolation model.

10.4.3 Relevant Finite-Element Kinematics

Finite-element discretization is achieved in the initial (reference) configuration by using either four or eight node isoparametric elements to interpolate the position of the element nodes, X_a, during deformation as

$$X = \sum_{a=1}^{n} N_a(\xi, \eta, \zeta) X_a \tag{10.16}$$

where $N_a(\xi, \eta, \zeta)$ are the standard shape functions defined in dimensionless element coordinates and n is the number of nodes (Fig. 10.9). During deformation the current position of the nodes, $x_a(x, y, z)$ as well as the nodal velocities, $\boldsymbol{v}_a$, can be expressed in terms of the shape functions as

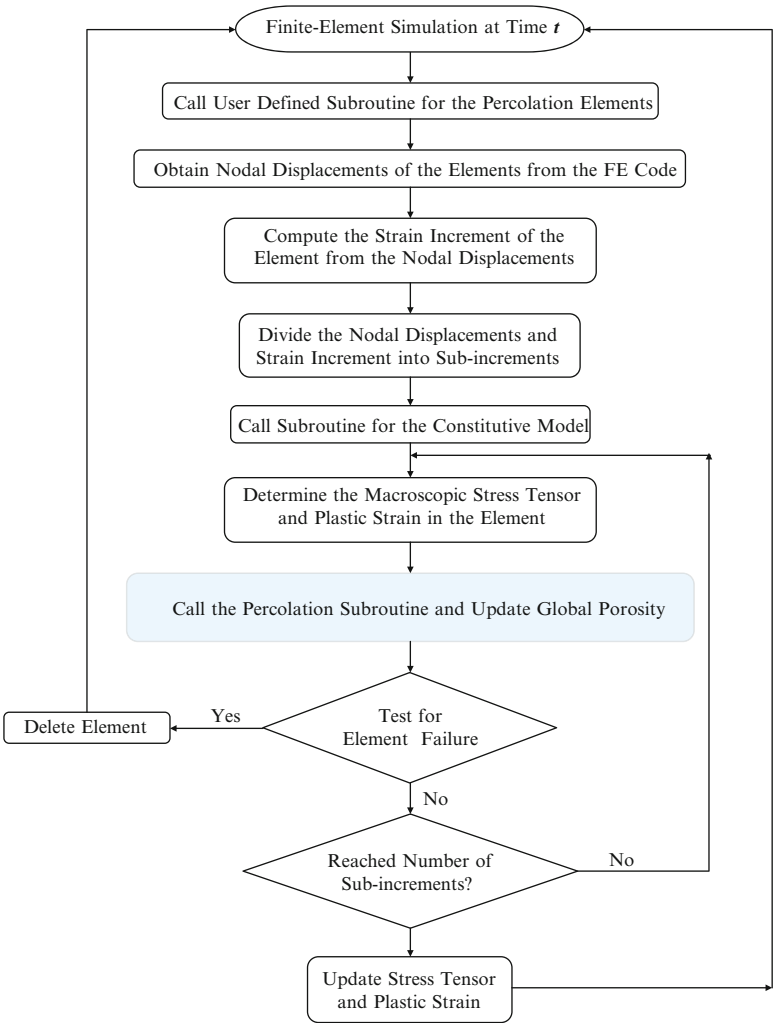

Fig. 10.8 Flow-chart of the macroscopic modeling process

$$x = \sum_{a=1}^{n} N_a x_a(t) \qquad v = \sum_{a=1}^{n} N_a v_a \qquad (10.17,\ 10.18)$$

By enforcing the displacement of the nodes by an arbitrary increment, $\boldsymbol{u}_{\mathrm{a}}$, the displacement can be interpolated as

$$u = \sum_{a=1}^{n} N_a u_a \qquad (10.19)$$

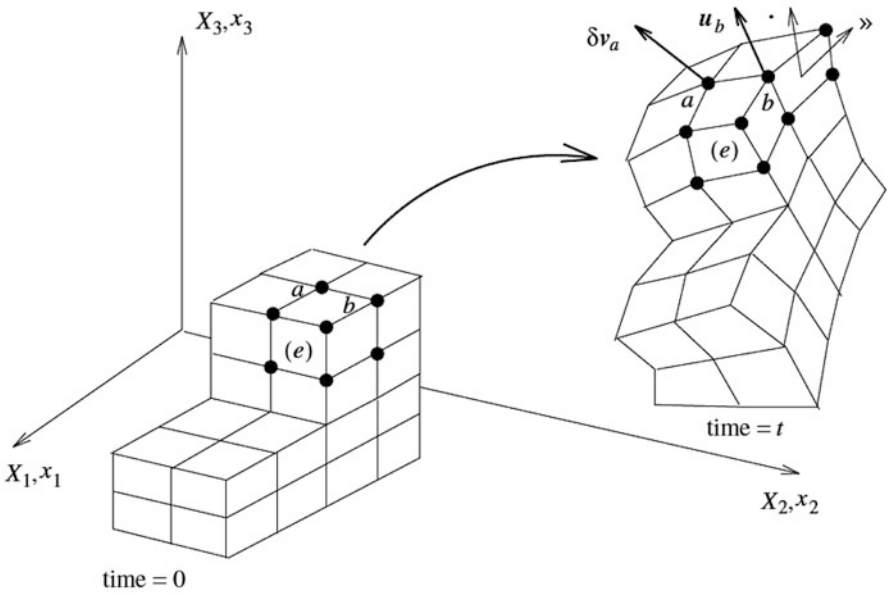

Fig. 10.9 Finite-element discretization (Reprinted with permission from Bonet and Wood (1997). Copyright 1997 Cambridge University Press)

The deformation gradient tensor, F, maps the element from its initial configuration to its deformed configuration and can be interpolated within the element using the relations

$$F = \sum_{a=1}^{n} x_a \otimes \frac{\partial N}{\partial x} \qquad \frac{\partial N}{\partial x} = J^{-1} \frac{\partial N}{\partial \xi} \qquad J = \sum_{a=1}^{n} x_a \otimes \frac{\partial N_a}{\partial \xi} \qquad \text{(10.20a, b, c)}$$

where J is the Jacobian matrix. The deformation gradient can be used to determine the strain measure of interest such as the Cauchy-Green strain. The strain matrix for specific elements will be discussed in a subsequent section.

The velocity gradient tensor, L, is related to the rate of change of the deformation gradient as

$$L = \dot{F} F^{-1} \tag{10.21}$$

The deformation gradient tensor can be decomposed into a stretch and rotation tensor. The rotational rate of deformation can be measured using the antisymmetric spin tensor, Ω, as

$$\Omega = \frac{1}{2}(L - L^T) \tag{10.22}$$

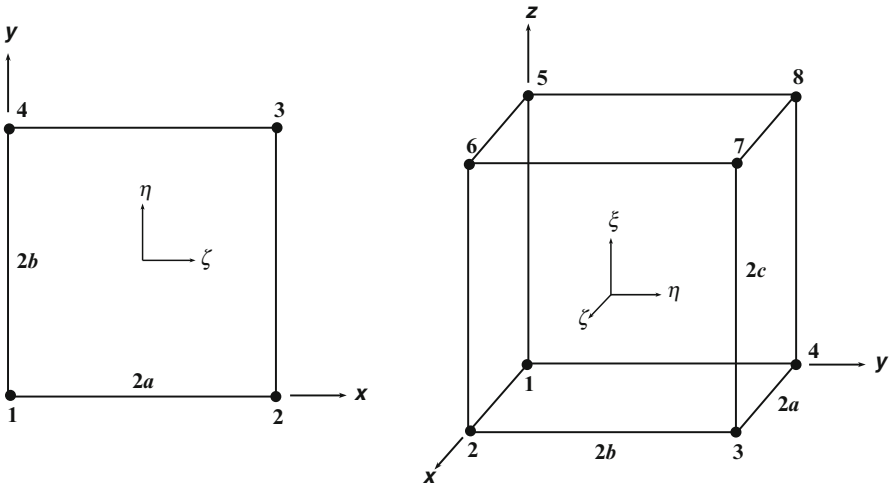

Fig. 10.10 Local node numbering and coordinate systems for a 4-node (*left*) and 8-node (*right*) isoparametric element

10.4.4 Percolation Element Types

The types of percolation elements considered are eight-node isoparametric brick elements and four-node isoparametric plane elements. The type of element integration such as reduced-point integration is controlled by the finite-element code. The geometry and local node numbering of the elements are shown in Fig. 10.10.

10.4.4.1 Eight-Node Isoparametric Brick Element

The geometry and local node numbering of the eight-node brick element is shown in Fig. 10.10. The center of the element is computed from the element nodal points as

$$x_c = \frac{1}{n}\sum_{a=1}^{n} x_a \tag{10.23}$$

where n is the number of element nodes. The half lengths of the element sides (a, b, c) are

$$a = \frac{1}{8}[(x_2 - x_1) + (x_3 - x_4) + (x_6 - x_5) + (x_7 - x_8)] \tag{10.24a}$$

$$b = \frac{1}{8}[(y_4 - y_1) + (y_3 - y_2) + (y_7 - y_6) + (y_8 - y_5)] \tag{10.24b}$$

$$c = \frac{1}{8}[(z_5 - z_1) + (z_6 - z_2) + (z_7 - z_3) + (z_8 - z_4)] \tag{10.24c}$$

Any point of interest within the element can be transformed to dimensionless element coordinates using the relations

$$\xi = \frac{x - x_c}{2a} \qquad \eta = \frac{y - y_c}{2b} \qquad \zeta = \frac{z - z_c}{2c} \tag{10.25a, b, c}$$

The shape functions for an isoparametric eight-node brick element at a node, a, are

$$N_a = \frac{1}{8}(1 + \xi_a\xi)(1 + \eta_a\eta)(1 + \zeta_a\zeta) \tag{10.26}$$

with derivatives

$$\frac{\partial N_a}{\partial \xi} = \left(\frac{\xi_a}{1 + \xi_a\xi}\right)N_a \tag{10.27}$$

The strain in the element can be interpolated using the shape functions. For an eight-node brick element, the macroscopic strain rate tensor is defined as

$$\dot{E}_{ij} = \begin{Bmatrix} \dot{E}_x \\ \dot{E}_y \\ \dot{E}_z \\ 2\dot{E}_{xy} \\ 2\dot{E}_{yz} \\ 2\dot{E}_{xz} \end{Bmatrix} = \sum_{a=1}^{n} \begin{bmatrix} \frac{\partial N_a}{\partial x} & 0 & 0 \\ 0 & \frac{\partial N_a}{\partial y} & 0 \\ 0 & 0 & \frac{\partial N_a}{\partial z} \\ \frac{\partial N_a}{\partial y} & \frac{\partial N_a}{\partial x} & 0 \\ 0 & \frac{\partial N_a}{\partial z} & \frac{\partial N_a}{\partial y} \\ \frac{\partial N_a}{\partial z} & 0 & \frac{\partial N_a}{\partial x} \end{bmatrix} \begin{Bmatrix} u_a \\ v_a \\ w_a \end{Bmatrix} = \sum_{a=1}^{n} \mathrm{B}_a u_a \tag{10.28}$$

10.4.4.2 Four-Node Isoparametric Plane Element

The relevant equations for a four-node isoparametric element can be readily determined from the equations for the eight-node element above by replacing the factor of 1/8 with 1/4 and setting any z-related quantities to zero. The strain rate tensor for the plane elements is slightly different and is written as

$$\dot{E}_{ij} = \begin{Bmatrix} \dot{E}_x \\ \dot{E}_y \\ \dot{E}_z \\ 2\dot{E}_{xy} \end{Bmatrix} = \sum_{a=1}^{n} \begin{bmatrix} \frac{\partial N_a}{\partial x} & 0 \\ 0 & \frac{\partial N_a}{\partial y} \\ 0 & 0 \\ \frac{\partial N_a}{\partial y} & \frac{\partial N_a}{\partial x} \end{bmatrix} \begin{Bmatrix} u_a \\ v_a \end{Bmatrix} + \begin{Bmatrix} 0 \\ 0 \\ \dot{\varepsilon}_z \end{Bmatrix} = \sum_{a=1}^{n} \mathrm{B}_a u_a + \dot{E}_z \tag{10.29}$$

where the strain increment in the z-direction (thickness direction) is not computed from the shape functions. If the element is a plane strain element then $\dot{E}_z = 0$. If the element is a plane stress element, then $\dot{E}_z$ will be iteratively determined during the stress integration routine to obtain the value of $\dot{E}_z$ that results in $\Sigma_z = 0$. Once the proper strain in the thickness direction has been determined, the component of the deformation gradient in this direction can be obtained. Assuming no shearing in the thickness directions, for a plane strain element, $F_z = 0$. For plane stress, the determinant of the Jacobian can be used to solve for F_z using the cumulative strains as

$$F_z = \frac{1 + E_x + E_y + E_z}{F_x F_y - F_{xy} F_{yx}} \tag{10.30}$$

10.4.5 Constitutive Model to Account for Material Softening

The percolation material model was written as a user-defined subroutine for LS-DYNA to integrate the stress state, analyze the microstructure for void evolution and return the stress tensor and plastic strain to the finite-element program. The extended Gurson-based yield criterion described in Chap. 4 with the calibrated q_2 parameter is used to account for material softening by using the global porosity, $\bar{f}_d$, and the average $\bar{q}_2$ value of the voids and cracks as

$$\Phi = \left(\frac{\Sigma_{\text{eq}}}{\bar{\sigma}}\right)^2 + 2\bar{f}_d q_1(\Sigma_{\text{hyd}}, \Sigma_{\text{eq}}, n) \cosh\left(\bar{q}_2 \frac{3}{2} \frac{\Sigma_{\text{hyd}}}{\bar{\sigma}}\right) - q_1^2(\Sigma_{\text{hyd}}, \Sigma_{\text{eq}}, n)\bar{f}_d^{\,2} - 1 = 0 \tag{10.31}$$

where

$$\bar{f}_d = \sum_{i=1}^{n_v} f_i^v + \sum_{i=1}^{n_c} f_i^c \qquad \bar{q}_2 = \frac{1}{\bar{f}_v} \sum_{i=1}^{n_v} f_i^v q_{2i}^v + \frac{1}{\bar{f}_c} \sum_{k=1}^{n_c} f_j^c q_{2j}^c \tag{10.32a, b}$$

with the subscripts v and c denote quantities for the voids and cracks, respectively, and an overbar symbol denotes a global quantity. The q_1 parameter does not require an averaging procedure since it is a function of the stress triaxiality and hardening exponent and these quantities are assumed to be homogeneous in the element.

10.4.6 Degradation of the Elastic Moduli

The elastic constants will degrade with the evolution of the porosity in the material and contribute to additional material softening. From a practical perspective, the porosity in most metals is too small to be a significant factor, but should be accounted for in the model for completeness. Since this is a secondary effect, the relations of Mori and Tanaka (1973) for spherical voids can provide a good approximation for the materials of interest and are well suited for random and clustered distributions of voids (Kachanov et al. 1994; Cramer and Sevostianov 2009). The degraded bulk and shear moduli of a voided material are expressed as a function of their initial values and the porosity as

$$\bar{\kappa}_d = \frac{4\bar{\kappa}(1-\bar{f}_d)\bar{\mu}}{4\bar{\mu}+3\bar{f}_d\bar{\kappa}} \qquad \bar{\mu}_d = \frac{(1-\bar{f}_d)\mu}{1+\bar{f}_d\left(\dfrac{6\bar{\kappa}+12\bar{\mu}}{9\bar{\kappa}+8\bar{\mu}}\right)} \tag{10.33a, b}$$

The elastic modulus and Poisson ratio can be computed from the bulk and shear moduli using the standard isotropic relations. The elastic constants of the average particle in the material are computed as a weighted average of the composition of each particle as

$$\bar{\mu}^p = \frac{1}{\bar{f}^p}\sum_{i=1}^{n_{pt}}\sum_{j=1}^{n_p} f_{ij}^p \mu_j^p \qquad \bar{\kappa}^p = \frac{1}{\bar{f}^p}\sum_{i=1}^{n_{pt}}\sum_{j=1}^{n_p} f_{ij}^p \kappa_j^p$$
$$\bar{f}_p = \sum_{i=1}^{n_{pt}}\sum_{j=1}^{n_p} f_{ij}^p \tag{10.34a, b, c}$$

where f_p is the total particle volume fraction and the subscripts i and j correspond to the particle type and particle number.

10.4.7 Global Coalescence and Failure of the Element

The onset of profuse void coalescence signalling failure of the particle field is easily identified because the voids will rapidly link-up throughout the field to form a single crack that encompasses the entire field. Failure of the particle field is identified by homogenizing all of the individual voids into an equivalent void and evaluating the coalescence model in Eq. (1.15) at each time-step. Since the porosity increases so rapidly at the onset of profuse coalescence, the choice of global failure criterion is not an important factor. Assuming a global failure porosity of 2 % as suggested by Chen (2004) for AA5182 sheet led to similar results identified by using Eq. (2.25) and by visual means. Ultimately, the coalescence criterion of

Pardoen and Hutchinson (2000) in Eq. (1.15) was adopted since it does not introduce any additional parameters into the model.

An additional advantage of this modeling treatment is that fracture is computed using the same procedure used in standard damage-based constitutive models. In this manner, the percolation model could be viewed as a sophisticated void evolution sub-model that is used in a standard Gurson-type model of ductile fracture. To compute the plastic limit-load for the global equivalent void, the void is assumed to be located at the center of the element and the element is treated as the unit cell. The global aspect ratio is computed as the weighted average of the voids and cracks in the material as

$$\bar{W} = \frac{1}{\bar{f}_v} \sum_{i=1}^{n_v} f_i^v W_i^v + \frac{1}{\bar{f}_c} \sum_{j=1}^{n_c} f_j^c W_j^c \tag{10.35}$$

The ligament spacing ratio of the global void is computed from the unit cell geometry as

$$\bar{\chi} = \left(\frac{\bar{f}_d \lambda_e}{\eta_{cell} \bar{W}} \right)^{\frac{1}{3}} \tag{10.36}$$

where $\eta_{cell} = \pi/6$ for a cubic unit cell and λ_e is the aspect ratio of the element with respect to the principal loading direction. The plastic limit-load criterion in Eq. (1.15) can now be evaluated using $\bar{W}$, $\bar{\chi}$, the principal macroscopic stress, Σ_1, and the material flow stress, $\bar{\sigma}$.

10.5 Microscopic Models

The micromechanical modeling procedure used in the percolation routine is presented in Fig. 10.11. The term 'microscopic' defines a quantity that is measured or defined within the element such as the equivalent plastic strain. At the macro-scale, the stress and damage are uniform and homogeneous and an equivalent void is used to account for material softening. Within the element at the micro-scale, the void and particle distributions are not homogeneous and vary within the element volume.

The microscopic models for void nucleation, growth, shape evolution and coalescence are detailed in Sects. 10.1, 10.2 and 10.3, respectively. At each time-step in the simulation and for each particle, void and crack, these sub-models are evaluated. The coalescence treatment is applied to each void/crack pair using the nearest neighbour information. The following sections will detail the kinematics for the voids, cracks and particles within each percolation element and the treatment used to identify the neighbouring objects and percolation elements.

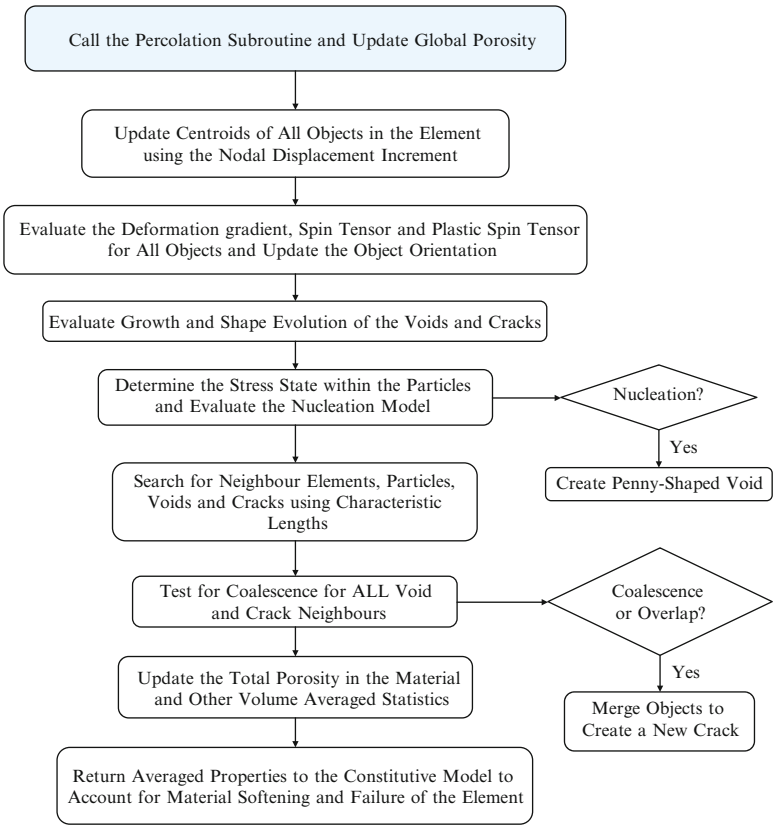

Fig. 10.11 Flow-chart of the percolation modeling process

10.5.1 Object Kinematics

10.5.1.1 Object Translation

The objects (particles, voids and cracks) will translate and rotate within the element during deformation. The location of the object is fixed within the dimensionless element coordinate system but its position will change in the global system as the element deforms as shown in Fig. 10.12. The centroids of each object are updated at each time step using the nodal displacements of the objects parent element and its shape functions evaluated at the object centroid. The position of the object center in the global system is calculated using Eq. (10.23).

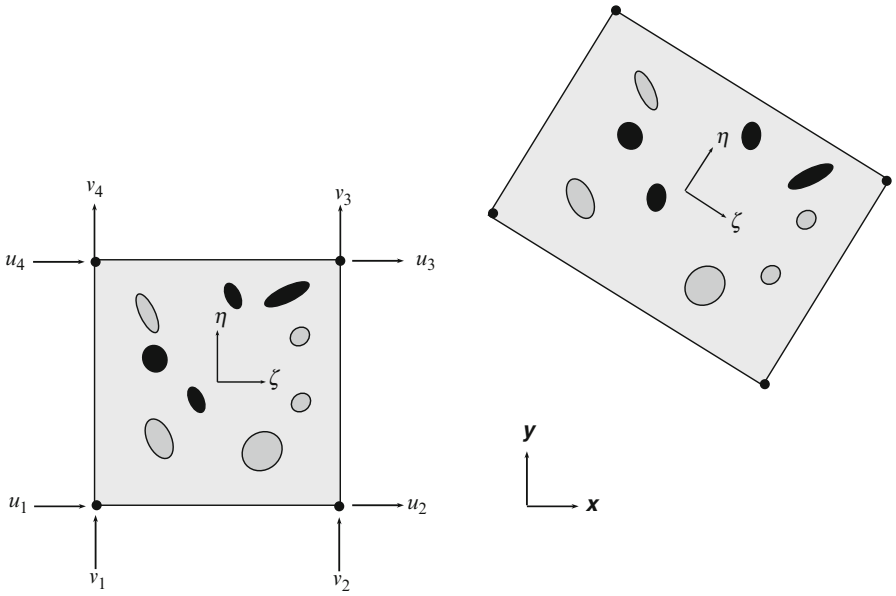

Fig. 10.12 Percolation element in the dimensionless element coordinate system (*left*) and in the global coordinate system (*right*) where the voids and particles have translated and rotated with the deformation of the element

10.5.1.2 Object Rotation

The rigid body rotation of the objects is computed from the material spin tensor of the element in Eq. (10.22). However, this rotation is not sufficient to describe the complete motion of the objects within the material as they may rotate due to plastic deformation within the element. In uniaxial tension, the material spin is zero but the objects will still rotate to align themselves with the principal loading direction. This effect should be considered because of its implications on the fracture mechanism because the objects will orient themselves to create favourable conditions for nucleation, growth and coalescence. Voids are more likely to coalesce when they are aligned transversely to the principal loading direction and particles will crack transversely to the loading direction. Particle and void rotation is especially important in torsion as shown in Fig. 10.13 where the voids and particles will rotate to align themselves at 45° to the loading direction.

The influence of plasticity-induced rotation has largely been neglected in the modeling of damage-induced ductile fracture. Typically, the voids have been assumed to remain stationary or to rotate with the material spin (Benzerga 2002; Pardoen 2006). More recent models by Keralavarma and Benzerga (2010) and Schyvaerts et al. (2011) have employed the nonlinear homogenization solution of Kailasam and Ponte Casteneda (1998) in its reduced form for voids as used by

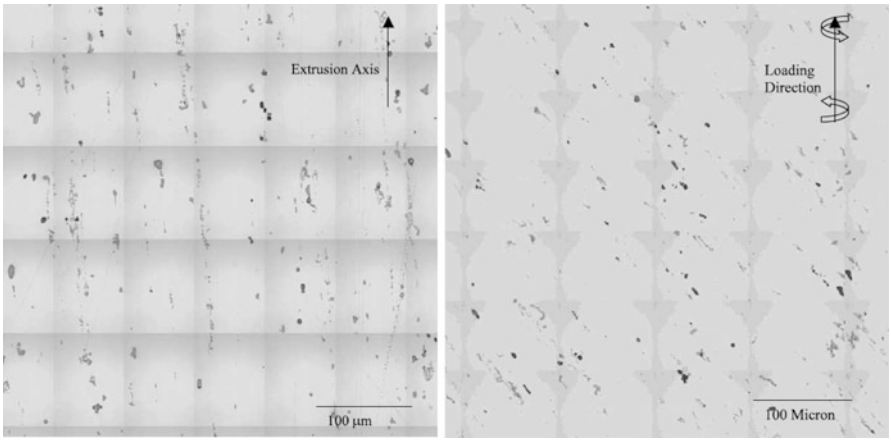

Fig. 10.13 Digitally compressed montage of 500 × 500 μm^2 area of an undeformed AA6061 alloy (*left*) and a montage after being subjected to a strain of 98 % in torsion (*right*) (Reprinted with permission from Agrawal et al. (2002). Copyright 2002 Elsevier)

Aravas and Ponte Casteneda (2004). These solutions are based upon a rigorous homogenization scheme to obtain expressions for the plastic spin rate in a composite material. This model has been shown to give very good agreement with the void rotation as validated by Schyvaerts et al. (2011) using finite-element simulations (Fig. 10.14).

The model of Kailasam and Ponte Casteneda (1998) will also be adopted to account for particle and void/crack rotations within the percolation element, albeit in a slightly reduced version. The solution of Kailasam and Casteneda (1998) can account for any number of different particle types in addition to the voids as well as their distributions. However, the computation of the spin rates requires many intermediate calculations of fourth-order tensors and matrix operations. With thousands of particles and voids within the percolation element and different particle types to be evaluated, this can be a computationally expensive process. Therefore, the rotation rate of each object type will be evaluated by neglecting interactions with the other object types, considerably reducing the expression for the rotation rate.

By also neglecting the distributional effects of the ellipsoidal objects within the material, the average deformation rate, D^{o}, and the average spin, Ω^{o}, of the local representative ellipsoidal object can be expressed as

$$D^{o} = A^{o} : \dot{E}^{p} \qquad \Omega^{o} = \Omega - \mathrm{C}^{o} : \dot{E}^{p} \qquad (10.37,\ 10.38)$$

Where Ω is the material spin rate of the element and $\mathbf{A}^{o}$ and $\mathbf{C}^{o}$ are fourth-order "concentration tensors" for the objects and are defined as

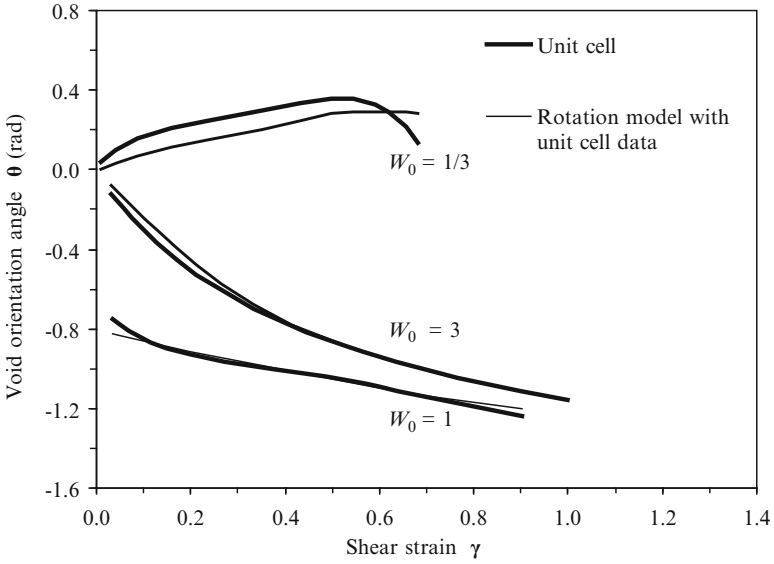

Fig. 10.14 Comparison of the analytical rotation model of Kailasam and Ponte Casteneda (1998) with the void rotation obtained from unit cell simulations (Reprinted with permission from Schyvaerts et al. (2010). Copyright 2010 Elsevier)

$$\mathbf{A}^{\mathrm{o}} = \left[\mathbf{I} - (1 - f^o)\mathbf{S}(\mathbf{I} - [\mathbf{L}^{\mathrm{M}}]^{-1}\mathbf{L}^o)\right]^{-1} \tag{10.39}$$

$$C^{\mathrm{o}} = (1 - f^o)\Pi^o\left[\left(\mathbf{L}^o - \mathbf{L}^{\mathrm{M}}\right)^{-1}\mathbf{L}^{\mathrm{M}} + (1 - f^o)\mathbf{S}\right]^{-1} \tag{10.40}$$

where f^o is the object volume fraction; $\mathbf{L}^{\mathrm{M}}$ and $\mathbf{L}^{\mathrm{o}}$ are the fourth-order viscosity (elastic) tensors of the matrix and object that are defined as a function of their shear and bulk moduli as $\mathbf{L} = (3\kappa, 2\,\mu)$. The fourth order tensors, $\mathbf{S}$ and $\mathbf{\Pi}$, are Eshelby tensors (1957) whose expressions are given in Butcher (2011). For the rotation of the voids and cracks, the expressions in Eq. (10.39) and (10.40) are computed by setting $L^o = 0$. In the limit that the object volume fraction approaches zero, the solutions reduce to those of Eshelby (1957).

The ellipsoidal object is defined as having semi-axes (a, b, c) where $a > b > c$ are corresponding vectors, $\mathbf{n}_1$, $\mathbf{n}_2$, $\mathbf{n}_3$. The microstructural spin, ω, in the global frame is defined as

$$\omega = \Omega^o + \frac{1}{2}\sum_{\substack{i,j=1 \\ i\neq j \\ w_i\neq w_j}}^{3} \frac{w_i^2 + w_j^2}{w_i^2 - w_j^2}\left[\left(\boldsymbol{n}_i\boldsymbol{n}_j + \boldsymbol{n}_j\boldsymbol{n}_i\right) : D^o\right]\boldsymbol{n}_i\boldsymbol{n}_j \quad (w_3 = 1) \tag{10.41}$$

where w_i are the aspect ratios of the object and are

$$w_1 = \frac{c}{a} \qquad w_2 = \frac{c}{b} \qquad w_3 = 1 \tag{10.42a, b, c}$$

Finally, the plastic spin of the object is expressed as

$$\Omega^p = \Omega - w \tag{10.43}$$

and the rotation rates of the semi-axes of the ellipsoid relative to the rotation of the continuum are

$$\dot{\boldsymbol{n}}_i = \Omega^p \boldsymbol{n}_i \tag{10.44}$$

The plastic spin will be zero if the material spin is zero and the object is aligned in the loading direction. Otherwise, the object will rotate until it is aligned with the principal loading direction. In the case that two of the aspect ratios are equal such as $w_1 = w_2$, Ω^p_{12} in Eq. (10.43) becomes indeterminate and is set to zero (Aravas and Ponte Casteneda 2004). If the object is spherical, the material is locally isotropic the plastic spin vanishes since $\mathbf{C}^{\circ} = 0$.

10.5.2 Implications of the Rotation Model on the Percolation Model

The adoption of the above rotation model significantly improves the physical foundation of the percolation model and has implications on void nucleation, growth and coalescence as these are all related to the direction of the maximum principal stress. During plastic deformation, the predictions of the rotation model are improved by computing the elastic tensor of the matrix, $\mathbf{L}^{\mathrm{M}}$, using the secant shear modulus, $\bar{\mu}_s$, determined as part of the homogenization process to determine the stress within the particles. In this manner, another level of integration is achieved in the percolation model.

The rotation model can be evaluated for the bulk values of each object type and applied uniformly to rotate each object within the particle field. However, this method neglects the individual object dimensions and any strain-gradients that exist within the element. This has been accounted for in the implementation of the model by evaluating the material deformation gradient, spin tensor and strain increment at the centroid of each object in the element using the equations in the previous section. The equations for the local plastic spin can then be determined using the above procedure by assuming that the local strain rate is a close estimate to the local plastic strain rate. This implementation provides an immense contribution to the model when shear loading is present as the shear-induced rotational distribution is captured by the model. Objects located in the center of the material will experience less rotation than the objects near the surface of the material where the shear

traction is applied. Overall, the treatment of particle and void rotation in the percolation model is physically sound and superior to the existing implementations of this model.

10.5.3 Neighbours – Element and Object

Since fracture is a local phenomenon originating within specific regions of the material, the spatial distribution of the neighbours of each object must be accounted for. This is accomplished by creating neighbour lists on the macro- and the micro-scale through the use of characteristic length parameters. If the distance from the centroid of an object to the centroid of a neighbour object is less than the characteristic length, it is appended to a neighbour list of that object. The size of the characteristic length controls the sphere of influence of the object. In the percolation model, up to four distinct characteristic lengths can be input to determine element neighbours, particle neighbours and void/crack neighbours.

At the global level, a characteristic length can be defined for the elements, L_e, to locate the neighbouring percolation elements and identify the objects within them for potential interactions (Fig. 10.15). This characteristic length is not a significant parameter except for crack propagation prior to final fracture as it enables the crack front to progress through neighbouring elements. For the most part, this parameter is used to reduce the number of interaction searches for each time step by limiting the size of the global neighbourhood. The simplest choice of selecting element neighbours is by using common nodes so that only the surrounding elements are considered. If more elements are required, the center-to-center distance between elements is used to identify the neighbours.

Within the global neighbourhood defined by the element length, up to three additional characteristic lengths can be adopted for:

Particle-particle neighbours: L_{pp}
Particle-void/crack neighbours: L_{pv}
Void-void, void-crack, or crack-crack neighbours: L_{vc}

It is important to have different characteristic lengths to be able to easily test for different interactions. For example, in modeling void nucleation within particle clusters, the particle-particle characteristic length will play a central role which is not likely to be the same as for void-crack interactions. The particle-void characteristic length could be used in modeling nucleation since the proximity of a particle to a crack will increase its propensity to nucleate a void. In the simplest case where no interactions are considered (isolated voids and particles) a single length can be used to define the local neighbourhood. In this case, any reasonable choice for this value such as five average diameters will be sufficient to identify the neighbouring particles, voids and cracks for nucleation and coalescence.

In the event of void coalescence, the new void inherits the neighbours of its parent particle and the new void is added to the lists of its neighbours. Similarly,

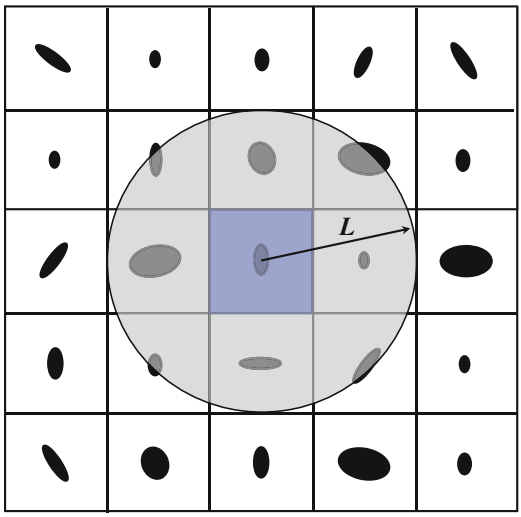

Fig. 10.15 Schematic of the identification process for neighbouring elements in an assemply of series of percolation elements at the continuum-scale where the voids within each percolation element have been homogenized into a single void located in the *center* of the element. This process is a natural analog to the non-local treatments of void damage

when two voids or cracks coalesce, the new crack will inherit the neighbour lists both parents and is added to these neighbours' lists as well. In this manner, coalescence will naturally sweep through the particle field, inheriting neighbours and coalescing with them as cracks propagate through the elements. The advantage of this method is that it is computationally efficient, physically sound, and relegates the characteristic length to a third-tier parameter. Of course, if the computational resources are available, every object within every element can be compiled into a neighbour list and no characteristic lengths are required.

10.6 Summary

Damage percolation modeling provides a unique tool to study and understand ductile fracture in heterogeneous materials. The present model has made significant in-roads into developing a physically sound framework to model fracture from first principles. The significant features of the present percolation model are:

- The model accepts a three-dimensional particle distribution of arbitrary ellipsoidal particles and voids.
- The particle fields are mapped to finite-elements to capture the development of the complex stress- and strain-gradients that develop in the microstructure.
- The initiation and evolution of damage at the micro-scale controls the bulk material behavior of the element and ultimately the structure in the finite-element model
- The Gurson-based yield criterion has been calibrated through the development of a library of correlations to model void evolution.

- The stress state within the particles is determined based upon a homogenization scheme and is a function of the particle shape, size and composition.
- A sophisticated void nucleation model for particle cracking is used to predict nucleation as a function of the particle stress (from homogenization theory), composition, fracture toughness, size and shape.
- Physically sound treatments for void growth, shape and coalescence have been developed that place no restriction on the void shape or orientation.
- The void growth, shape evolution and coalescence models have been calibrated and validated from an extensive study of voided unit cells.
- An advanced rotation law based upon homogenization theory has been adopted to account for the plastic spin of the particles, voids and cracks within the material.
- No material calibration parameters are required by the model or have been introduced. All parameters are directly related to the material such as the particle composition, flow stress relation of the matrix, etc. The only parameter that could be calibrated with experiment would be the fracture toughness of the particles if it cannot be predetermined. Otherwise fracture is a natural consequence of microstructure evolution.

The theoretical development of the percolation model concludes with this chapter. The subsequent chapters will develop a particle field generator to populate the percolation elements with statistically representative particle fields. Finally, the complete finite-element percolation model will be evaluated in Chap. 11 to predict damage initiation and failure in an aluminum-magnesium alloy.